The Impact of Ice Formation on Wind Turbine Performance and Aerodynamics

Article *in* Journal of Solar Energy Engineering · February 2011

DOI: 10.1115/1.4003187

4 authors, including:

Sarah Barber
University of Applied Sciences of Eastern Switzerland
53 PUBLICATIONS **483** CITATIONS
SEE PROFILE

Soleil Jafari
Islamic Azad University, gonbad Branch
10 PUBLICATIONS **176** CITATIONS
SEE PROFILE

Ndaona Chokani
ETH Zurich
92 PUBLICATIONS **1,329** CITATIONS
SEE PROFILE

European Wind Energy Conference (EWEC 2010)

The Impact of Ice Formation on Wind Turbine Performance and Aerodynamics

S. Barber
barbers@ethz.ch

Y. Wang
wang@lec.mavt.ethz.ch

S. Jafari
jafari@lec.mavt.ethz.ch

N. Chokani
chokani@lec.mavt.ethz.ch

R.S. Abhari
abhari@lec.mavt.ethz.ch

Laboratory for Energy Conversion, ETH Zürich MLJ33, Sonneggstrasse 3, 8092 Zürich, Switzerland
T: +41(0) 44 632 6834 / F: +41(0) 44 632 1100

Abstract:

Experimental and computational studies are undertaken to examine the effects of ice formation on wind turbine performance. The experiments are conducted on a dynamically-scaled model in the wind turbine test facility at ETH Zurich. The central element of the facility is a water towing tank that enables full-scale non-dimensional parameters to be more closely matched on a sub-scale model than in a wind tunnel. A novel technique is developed to yield accurate measurements of wind turbine performance. These measurements are complemented by predictions obtained using a commercial Reynolds-Averaged Navier-Stokes Computational Fluid Dynamics code. The results show that icing typical of that found at high altitude (2,330 m) can reduce the power coefficient by up to 22% and Annual Energy Production (AEP) by up to 2%. Icing in the blade tip region, 95-100% span, has the most pronounced effect on the performance. For wind turbines in more extreme icing conditions, icing can result in up to 17% losses in AEP. Icing at high altitude sites does not cause significant AEP losses, whereas icing at lower altitude sites can have a significant impact on AEP. The classification of icing is thus key to further development of prediction tools. It would be advantageous to tailor blade heating for prevention of ice build-up on the blade's tip region. An "extreme" icing predictive tool for the development of wind farm projects in regions that are highly susceptible to icing would be beneficial to wind energy developers.

Keywords: wind turbine, wind, energy, performance, icing, measurement, simulation.

1 Introduction

1.1 Background

Wind energy is the world's fastest growing source of electricity production and a key source of clean, plentiful energy for the future. In order for wind energy to more fully reach its potential, sites with a rich wind resource must be effectively taken advantage of. As the power output of a given wind turbine is proportional to the cube of the wind velocity, a site's capacity is highly dependent on the wind speed. Many favourable sites for wind farms in terms of high wind speeds are located in cold, wet regions such as the Swiss Alps, the northern Scandinavian coastline, many areas of China, Northern USA and Canada. In these regions the installation of wind turbines is limited due to problems of ice formation, both on instrumentation and on the blades. Predicted power curves can be of low accuracy, and the actual performance often deviates significantly from the expected performance [1]. This difference between the actual and predicted power curve arises due to the effects of icing, high turbulence and gusts among other sources. The present paper focuses on the effects of icing. The improved understanding and quantification of these losses is vital for wind farm developers and investors, who must estimate accurately the expected energy production of a project in order to quantify its risks and assess its financial viability.

The formation of ice on airfoils is generally known to have a detrimental effect on their lift coefficient (C_L) and drag coefficient (C_D) performance. Icing on aircraft wings has been well documented, using icing wind tunnels [2] and numerical simulation [3]. C_L was found to reduce by up to 30% and C_D was found to increase up to 50%. The effect of icing on wind turbine blades has been less

studied [4]. Power losses due to icing have been estimated to be up to 20% using 2D Computational Fluid Dynamics (CFD) and Blade Element Momentum (BEM) methods [5].

1.2 Aim and objectives

The present work is a combined experimental and computational study on the effect of icing on wind turbine performance and aerodynamics. The work is unique in several respects. First the experiments are conducted on a dynamically-scaled model at near full-scale non-dimensionals; thus the results are applicable to full-size wind turbines. Secondly the experiments involve the application of a novel power measurement method in order to accurately assess the differences in performance due to icing. Furthermore the computations are used in conjunction with the experiment to explain the effect of icing on performance. The specific objectives of the work are threefold; to quantify the impact of icing on the performance of wind turbines; to explain the source of this impact; and to propose practical approaches to mitigate the adverse effects of icing. This will help to understand the effects of icing on wind turbine performance and allow the production of recommendations for improved performance in icing conditions. The remainder of the paper discusses the set-up of the experimental and the computational parts, followed by a presentation of the results for each part and a discussion at the end.

2 Set-up

In this work, the performance of a three-bladed scale-model wind turbine was investigated experimentally in a water towing facility and computationally using a Reynolds-Averaged Navier-Stokes solver. The aluminum blades (Figure 1 (a)) matched the S809-profile, tapered and twisted blades of the NREL Phase VI rotor from 25% to 100% span [6]. From the hub to 25% span the blade profile was modified in order to improve the structural rigidity. The hub size was 0.18*R* compared to the NREL hub of 0.14*R*, where *R* is the rotor radius. The effects of icing were investigated by attaching simulated ice shapes to the blades.

2.1 Definition of ice shapes

The ice shapes were defined to approximate the shapes obtained from analysis of the photographs from in-situ full-scale wind turbines with icing and from the results of numerical simulations using an ice accretion code. The shapes studied in this work are summarised in Figure 1(b). The span-wise distribution refers to the span-wise extent of icing measured from the blade tip.

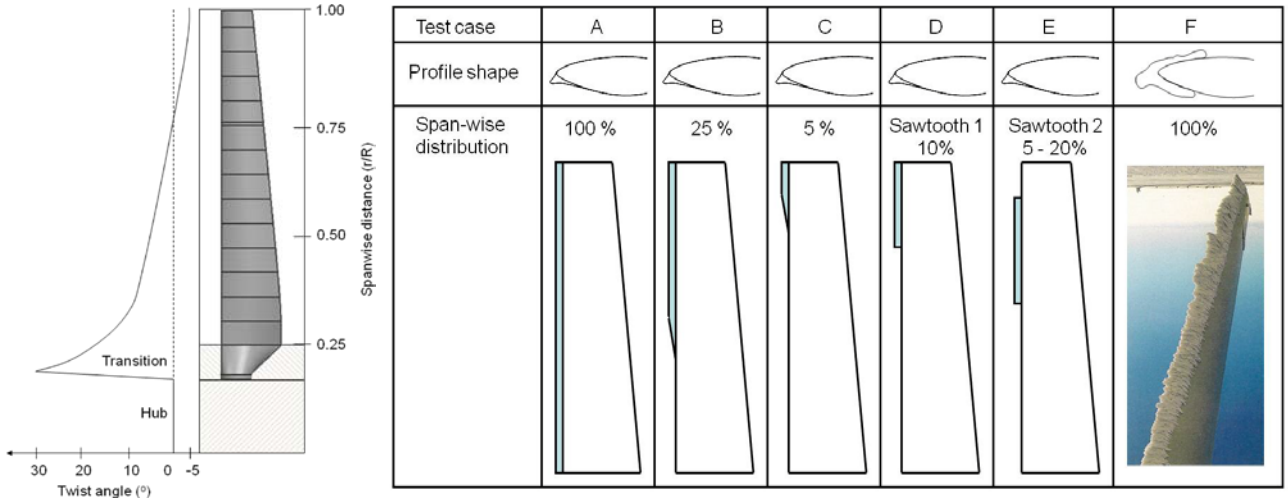

(a) (b)

Figure 1: (a) the blade design, (b) defined ice shapes.

The photographs provided the span-wise distribution of ice accumulation and served as a reference for the validation of simulated ice shapes. The 2D NASA-LEWICE ice accretion code was used to provide 2D ice profiles. This combined use of photographs and ice accretion code thus enabled the detailed 3D ice shapes to be reproduced. LEWICE was used to predict 2D ice profile shapes on the blades at eight different span-wise locations. The parameters used in this ice accretion code, as shown in Table 1, were selected using the conditions at the Alpine Test Site Gütsch (Switzerland), at which there is a 600 kW Enercon E40 wind turbine.

Turbine diameter	44 m
Turbine rotational speed	15 rpm
Wind velocity	4 m/s
Temperature	-6 ^{o}C
Liquid water content	0.1 g/m^{3}
Droplet diameter	35 □m
Icing duration	10 hours

Table 1: parameters used to define icing profiles.

The atmospheric conditions were taken as the average values over a year of data measured on the turbine and at a nearby metrological station between the dates 01.06.2007 and 31.05.2008 (from Meteotest). In order to estimate the liquid water content, simulations using the Weather Research & Forecasting model [7] were carried out by Meteotest for a typical icing event at Gütsch. The chosen droplet diameter was estimated based on previous LEWICE simulations [3].

The LEWICE results for span-wise distances r/R = 0.30, 0.63 and 0.90 are shown in Figure 2 (a). The shape grows with increasing span due to the increasing rotational ($r\omega$) component of the velocity and decreasing angle of attack (α). The results from LEWICE were used in conjunction with photographs from the Alpine Test Site Gütsch. Approximately 11,000 photographs from a camera mounted on the nacelle of the wind turbine taken over the period between 01.06.2007 and 31.05.2008 were analysed to establish typical span-wise distributions. It should be noted that the blades on the turbine at Gütsch are fitted with air heating systems, which are activated if the power output reaches unacceptably low values in cold temperatures. This means that the ice profiles are not extreme.

Once span-wise ice distributions were established and the 2D profile shapes were predicted in LEWICE, five ice shapes (Cases A – E) were defined for the tests. Cases A-C represent varying length of span-wise ice formation, which result from the varying tip speed ratio conditions of the wind turbine. In each case, the ice shape was linearly tapered to avoid sharp steps. Cases D and E represent the "saw-tooth" effect that was frequently observed in the photographs. This occurs when parts of the ice falls off the blade during motion. These shapes were made intentionally with sharp steps. An example photograph from Gütsch is shown in Figure 2 (b) compared to the CAD drawing for Case A. The view angle is the same as the camera angle. The final ice shape (Case F) is an extreme case that was not observed at Gütsch, but at a site where no heating system is present (e.g., Grenchenberg, Switzerland).

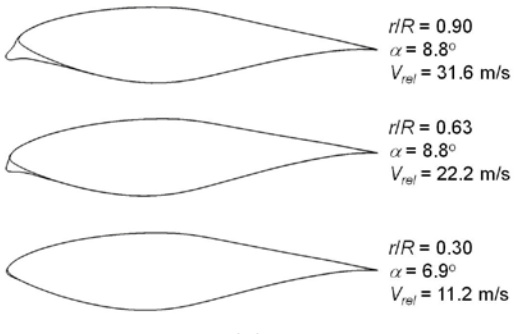

(a)

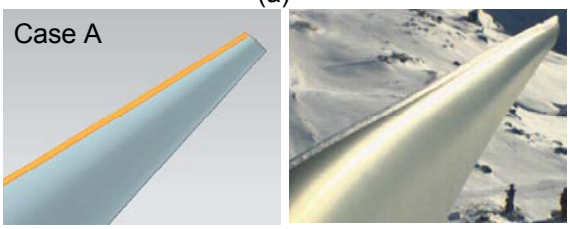

(b)

Figure 2: (a) predicted ice profiles at 3 span-wise locations, (b) comparison with photo from Gütsch.

2.2 Experimental set-up

The experimental work was carried out in the sub-scale model wind turbine test facility at the Laboratory for Energy Conversion (LEC) of ETH Zürich (Figure 3 (a)). The test facility comprises a 0.3 m diameter wind turbine model that is mounted on a carriage that moves above a 40 m long, 1 m wide and 1 m deep channel of water. The velocity of the carriage can be specified to up to 3 m/s (± 1%), as shown schematically in Figure 3 (b).

(a)

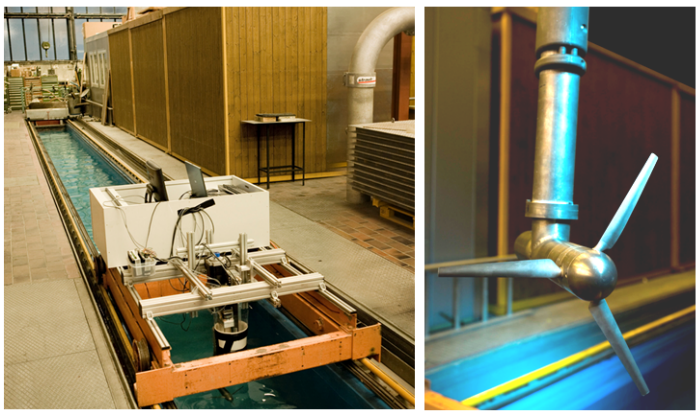

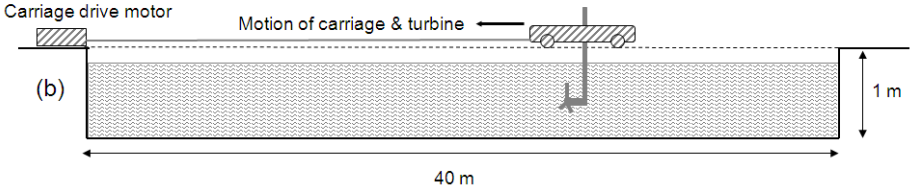

Figure 3: LEC's sub-scale model wind turbine test facility, (a) photograph, (b) schematic diagram.

The water temperature is at 19 ^{o} ± 0.5 ^{o} throughout the measurement campaign. The rotor is placed in the centre of the channel and the blockage ratio ($A_{rotor}/A_{channel}$) of the model is 7.1%, which is below the upper limit of 7.5% that is required to apply blockage corrections [8]. The Froude number of the channel ranges from 0.03 up to 0.92 for the maximum velocity of 3 m/s. Thus surface and blockage effects have a negligible effect on the wind turbine performance.

The rotor blades are interchangeable and the pitch angle can be set with an accuracy of ± 1 ^{o}. For the current tests the blade pitch was 0 ^{o} following systematic tests to find the pitch giving the optimal C_P curve. The rotational speed of the wind turbine is controlled by a brushless motor. The desired tip speed ratio of the wind turbine can thus be accurately specified. In this study, the turbine rotational speed was kept at 800 rpm (± 3 rpm), which avoided cavitation on the blades. The tip speed ratio was varied from 5 to 8 by varying the carriage velocity between 1.5 and 2.8 m/s.

The Reynolds number based on mean chord at the optimal tip speed ratio of 6.0 is about 1.5 x 10^5 in this facility. As a comparison, the same size model in a wind tunnel with the same free-stream flow conditions would have a Reynolds number of 10,000. The largest wind tunnel facility used for wind turbine testing (at NASA-AMES) has Reynolds numbers of the order of 1.0 x 10^6. At the Alpine Test Site Gütsch the Reynolds number is approximately 4.0 x 10^6. It is evident that this facility enables the full-scale non-dimensional parameters to be better duplicated on the sub-scale model than in air.

To determine the performance of the wind turbine, an in-line, contactless miniature torque-meter with measurement range 0-5 Nm (accuracy ± 0.1%) wasinstalled on the shaft. Torque was converted to power by multiplying it by the rotational speed. The power of the turbine, P_{turb}, measured in the water channel, is comprised of the power required by the motor to overcome friction in the drive-train, P_{drive}, the dynamic sealing, P_{seal}, and the power absorbed by the rotor itself, P_{rotor}, which is negative for a wind turbine:

$$P_{turb} = P_{drive} + P_{seal} + P_{rotor} \quad (1)$$

Or for constant rotational velocity, ω:

$$T_{turb} = T_{drive} + T_{seal} + T_{rotor} \quad (2)$$

where T = torque (N/m^2). As shown in Figure 4, the measurement of T_{turb} in the water channel requires also a series of tare measurements in order to determine T_{drive} and T_{seal}. This approach assumes that the parasitic torque components due to the seal and the housing are decoupled from each other and from the torque produced by the blades. Once T_{rotor} was established for each case, the power coefficient was determined as follows:

$$C_P = \frac{T_{rotor}\omega}{\frac{1}{2}\rho V^3 A_{rotor}} \quad (3)$$

where A_{rotor} is the cross-sectional area of the rotor (m^2), V the carriage velocity (m/s) and ρ the fluid density (kg/m^3). The relative errors of the C_P and tip speed ratio measurements arise from the errors in the translational velocity (± 1%), rotational velocity (± 0.4%), torque (± 0.1%) and water temperature (± 0.2%). The worst case relative errors were found to be 3.0% in C_P and 1.1% in tip speed ratio.

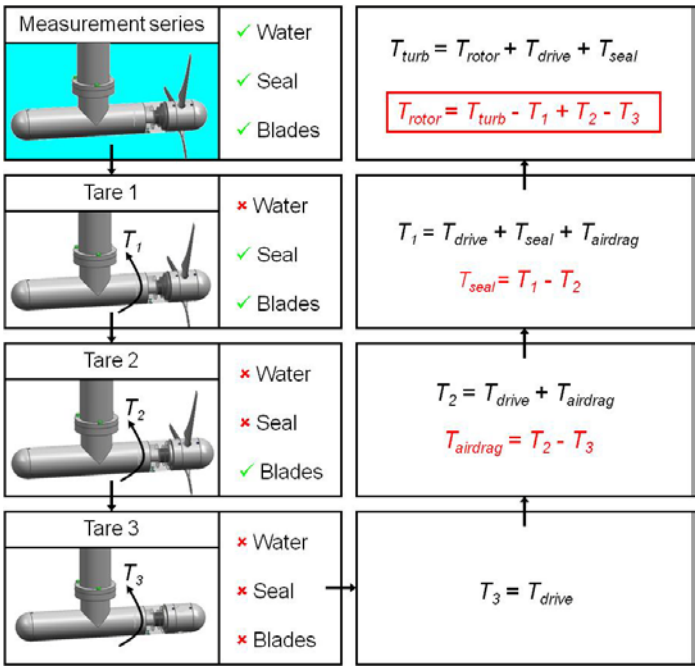

Figure 4: torque measurement method.

2.3 CFD simulations

The commercial code ANSYS CFX 11.0 was used to perform the CFD analysis. A single blade was analysed with periodic boundaries as shown in Figure 5.

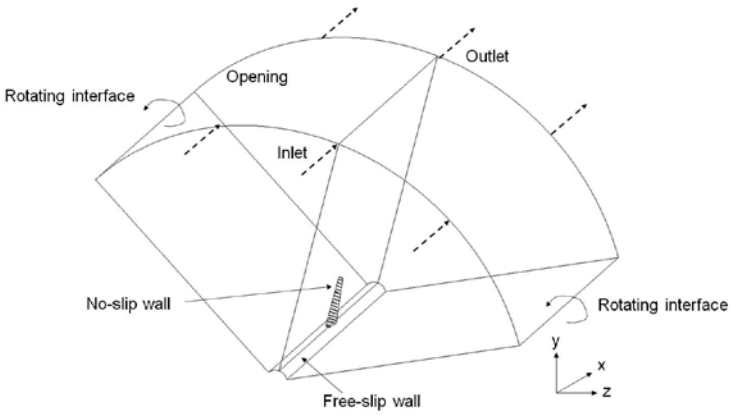

Figure 5: computational domain.

To reduce the computational requirements, the study was limited to a 120 ^{o} arc-shaped domain of radius 4*R* and length 4*R*. An unstructured tetrahedral mesh was constructed in the domain with 10 prism layers on the surface of the blade. It was ensured that at least 10 cells were in the boundary layer, a requirement for the use of the scalable wall function with the *k*-ε turbulence model. The y^+ value on the blade surface was in the range 30 to 60. A denser region of cells was constructed in the rotor wake. The grid dependency study included altering the cell sizes on the boundary surfaces region, the wake region and in the prisms close to the blade surface, until grid independent solution was found. The resulting mesh contained approximately 4 million cells. Convergence was considered adequate once the average residuals had decreased by five orders of magnitude. As in theexperiment, the rotational speed of the rotor was 800 rpm and the inlet velocity was varied. The boundary conditions and solution methods are summarised in Table 2.

Boundary conditions	
Inlet	Inlet v = 1.6 – 3.1 m/s
Outlet	Outlet constant pressure
Top	Opening constant pressure
Bottom	Wall free slip
Blade	Wall no slip
Periodic boundaries	800 rpm

Table 2: CFD boundary conditions.

3 Results

3.1 Experiments

Reynolds number correction

As noted above, the dynamically-scaled model in the present work better duplicates the full-scale Reynolds number than in a wind tunnel. However the measured power coefficient must be corrected to account for the Reynolds number difference between the sub-scale model and a full-scale turbine. A Reynolds number correction was therefore developed as described next.

As shown in Section 2.2, the power coefficient can be calculated if the torque acting on the rotor is known. The torque acting on a wind turbine blade can be calculated, for example using Blade Element Momentum (BEM) codes, by integrating the torque acting on a finite number of discrete elements along the span of the blade, given by:

$$\delta T = \delta L \cos(\alpha + \beta) + \delta D \sin(\alpha + \beta) \qquad (4)$$

where α = effective angle of attack (^{o}) and β = blade twist (^{o}) at the given element location. The integration of these torque values requires knowledge of the C_L and C_D at a range of angle of attacks for the airfoil, and BEM codes usually require independently measured C_L and C_D vs. α data for the relevant Reynolds number as an input. For the current airfoil and operating conditions it was calculated from BEM that the effective angle of attack remains lower than 10^{o}. As the lift slope in the non-separated, lower-α regime is not affected by viscous effects [9], C_L in this work is not expected to be significantly affected by Reynolds number. The changes in torque, and therefore power coefficient, at different Reynolds numbers, are thus only affected significantly by C_D. Furthermore, due to the low effective angle of attack operating range of the airfoil, C_D is dominated by skin friction drag. The skin friction coefficient for turbulent flow (c_{fT}) over a flat plate is defined as follows [10]:

$$c_{fT} = \frac{0.074}{\mathrm{Re}_T^{0.2}} \qquad (5)$$

where Re_T is the local blade Reynolds number. Thus the corrected power coefficient is estimated as follows:

$$C_P = \frac{c_{f\mathrm{Re}'}}{c_{f\mathrm{Re}}} C_P' \qquad (6)$$

where C_P' is the uncorrected power coefficient, *Re* the full-scale Reynolds number and *Re'* the sub-scale Reynolds number. A comparison of measurements of a 2-bladed sub-scale model in the ETHZ facility (*Re'* = 1.44 x 10^5) and the NREL Phase VI test case [11] (*Re* = 9.06 x 10^6) is shown in Figure 6. The two measurements have an average difference of 5%, which confirms the applicability of the Reynolds number correction that is developed here. The differences at lower tip speed ratios are attributed to separation effects that are not accounted for and to 3D effects that could arise from the slightly larger hub.

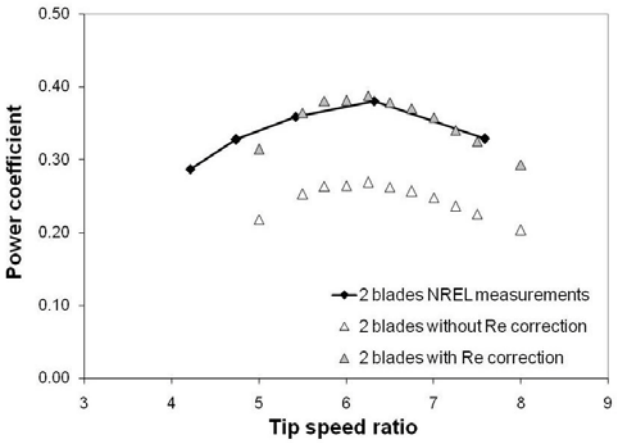

Figure 6: power coefficient vs. tip speed ratio validation (2-bladed rotor).

Power coefficient curves

The power coefficient vs. tip speed ratio curve for two tests of the 3-bladed rotor with clean blades (no ice) is shown in Figure 7. The curve is as expected for a 3-

bladed wind turbine [12], with optimum performance at a tip speed ratio of approximately 6.0 – 6.5, where the power coefficient is 0.47. The repeat measurements show very good repeatability and a maximum variation in C_P of 1.7%, which is within the relative error of the experiment (Section 2.2).

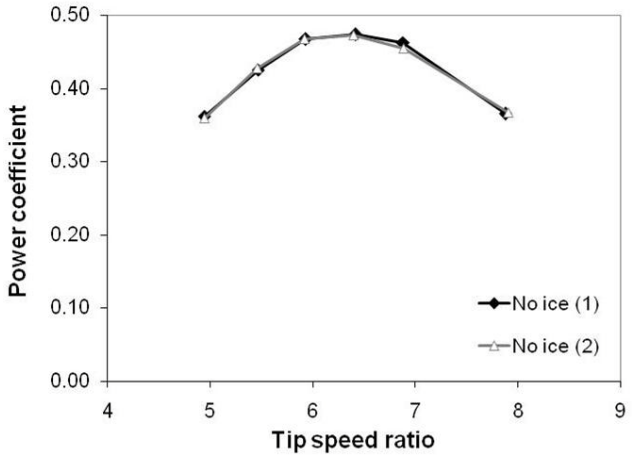

Figure 7: power coefficient vs. tip speed ratio graph, 3-bladed rotor with no ice, experiment.

The effect of icing on the wind turbine performance is shown in Figure 8 (a) for Cases A, B & C and (b) for Cases D, E & F. Additionally, the relative magnitudes of C_P are examined further in Figure 9, in which ΔC_P (the difference between C_P with ice and C_P with no ice) for the Cases A-E for three tip speed ratios are compared. Case F is not included for sake of clarity.

It can be seen that the presence of the ice generally has a detrimental effect on the performance of the rotor. The reduction of C_P is as large as 0.08 (or 29.3%) for Cases A and B. The effect is smaller at lower tip speed ratios, and all the C_P values are within 0.015 of each other at a tip speed ratio of 4.9. This trend is expected because the losses at high tip speed ratio are mainly dictated by the aerodynamic drag of the blades, whereas the losses at low tip speed ratio are dominated by the wake angular momentum losses. The aerodynamic drag of the blades is expected to be altered due to the ice shapes, whereas the wake losses are less sensitive to blade profile and tip speed ratio. Thus the ice shapes are expected to alter C_P more significantly at higher tip speed ratios. On examination of the uniform ice shapes (Cases A-C), it can be seen that C_P is reduced by up to 29.3% (at tip speed ratio = 7.9) for the 100%-span ice shape (Case A). The 25%-span ice shape (Case B) shows very similar behavior, the maximum difference from Case A being 2.6% at tip speed ratio = 7.9. This suggests that only the ice in the outboard 25% of the span has a significant effect on performance. Furthermore the reduction in performance measured for the 5% case (Case C) is approximately half that of the 25% case for the tip speed ratios close to the maximum. This means that the presence of ice on the outboard 5% of the blade has a similar impact on performance as ice on 75% to 95% of the span. This indicates a rapidly increasing effect on performance from ice that is nearer the tip. Thus ice removal or prevention systems could be substantially more efficient if their effectiveness was tailored to the outboard 5% span of the blades. Cases D and E show the effects of the two "sawtooth" shapes on the turbine performance. Ice Case D consists of one sharp step from the ice shape to the blade surface at 10% span. This has a very similar effect on performance as the 5% span tapered ice shape (Case C). Case E has two sharp steps from the blade to the ice shape on either side at 5% and 25% span. This ice shape has a larger influence on C_P at high tip speed ratios (C_P is 7.4% larger for Case E than for Case D at a tip speed ratio of 6.9). This again highlights the strong effect of ice that is on the outboard 5% span.

The extreme ice shape, Case F, has a major effect on the C_P. No power is generated for tip speed ratio > 6, and the power is small for tip speed ratio < 6.

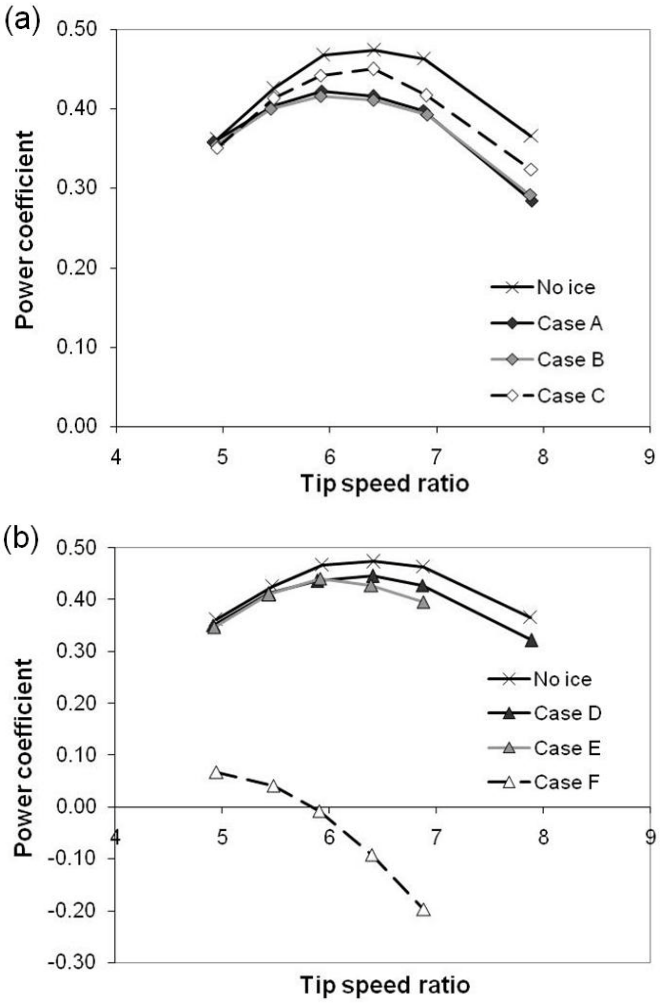

Figure 8: power coefficient vs. tip speed ratio graph for the rotor with ice shapes attached to blades: (a) cases A-C compared to no ice case, (b) cases D-F compared to no ice case.

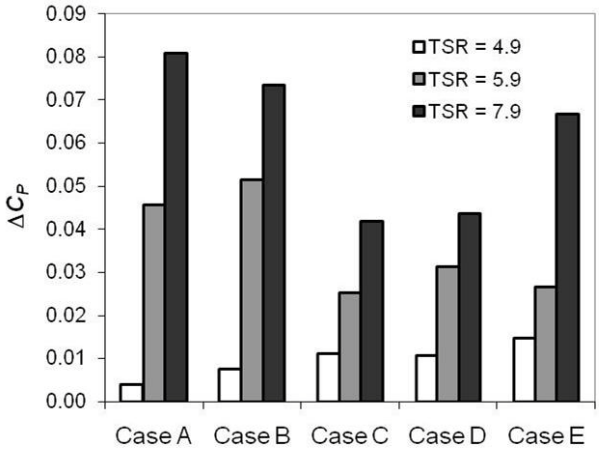

Figure 9: ΔC_P for Cases A-E for three tip speed ratios.

Annual Energy Production

The potential effects of the ice shapes on the corresponding Annual Energy Production (AEP) of a wind turbine were estimated using the atmospheric conditions at the Alpine Test Site Gütsch and specifications of its wind turbine. A continuous operation at a tip speed ratio of 5.9 (and thus the corresponding C_P measured in the above experiments) was assumed. The resulting power curves for the no ice case and for Case A are shown in Figure 10, where the air density was taken as the average at the Alpine test Site Gütsch of 0.9757 kg/m^3 and the curve was cut off at the rated power of 600 kW to simulate pitch control.

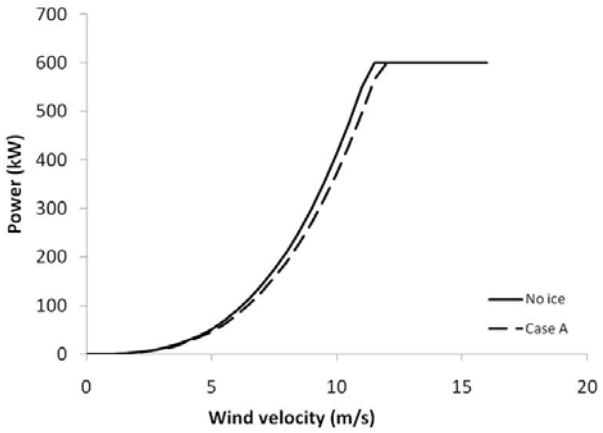

Figure 10: estimated power curves for the no ice case and Case A.

The AEP was estimated using the IEC standard bins method [13], where $\varepsilon(v)$ = power curve and $f_{ref}(v)$ = measured wind speed frequency distribution over a year at the test site Gütsch:

$$AEP = \int_0^\infty \varepsilon(v) f_{ref}(v) du \qquad (7)$$

The resulting AEP for each case is summarised in Table 3, for icing 100% of the time and for icing for only two months of the year. The two month long period was estimated as the duration of likely ice formation based on temperature data measured at Gütsch over a year together with LEWICE simulations for a range of temperatures and humidities.

	12 months icing		**2 months icing**	
Case	AEP (MWh)	% loss	**AEP (MWh)**	**% loss**
Clean	181	-	**181**	**-**
Case A	163	9.7	**178**	**1.6**
Case B	161	11.0	**177**	**1.8**
Case C	171	5.4	**179**	**0.9**
Case D	169	6.7	**179**	**1.1**
Case E	170	5.7	**179**	**0.9**
Case F	0	100	**151**	**16.7**

Table 3: effect of ice on Annual Energy Production.

In a separate study [1] the actual loss in AEP at Gütsch due to ice formation over a year was estimated to be approximately 1.1%, which is good general agreement with Cases A-E. Case F, which is representative of ice formation for example in the Bern Jura, clearly has a much more deleterious effect (17% less) on the AEP. Such an ice shape would lead to increased blade loading and possibly a loss of aerodynamic damping, which would reduce the lifetime of the blades and gearbox. This would also have to be considered in a full cycle lifetime analysis.

3.2 CFD Simulations

The steady-state results of the CFD simulations are presented next. For the examination of the performance due to the ice shapes, the behavior at a tip speed ratio of 6.0 was considered. This operating point is the main region of interest particularly for variable speed wind turbines as at Gütsch. The C_P results were corrected for Reynolds number as in Section 3.1. In Figure 11 the predicted ΔC_P values for Cases A-E (tip speed ratio = 6.0) are compared to the experiment (tip speed ratio = 5.9). The case-to-case trends in the predictions match the experiment well for all cases (within a ΔC_P value of 0.009 of each other, or 2.5% of the measured C_P). Case F reduces C_P to zero in both cases (100% loss).

The predicted streamlines, Figure 12, show that there is no significant difference between the streamlines for the blade with no ice and for Case A and thus Case A does not significantly alter the characteristics of the flow separation. The only region of flow separation is at the hub. This flow behavior was also observed for Cases B-E, and explains why the measured C_P values are all of the same order. However, Case F has massive amounts of separation across the span. This explains the total loss in power seen for this tip speed ratio for Case F.

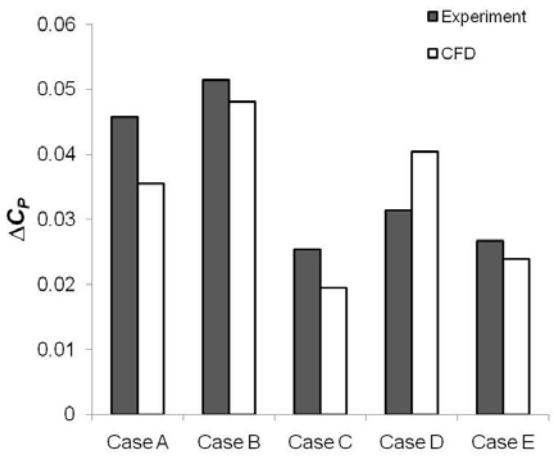

Figure 11: ΔC_P for Cases A-E for CFD (tip speed ratio = 6.0) and experiment (tip speed ratio = 5.9).

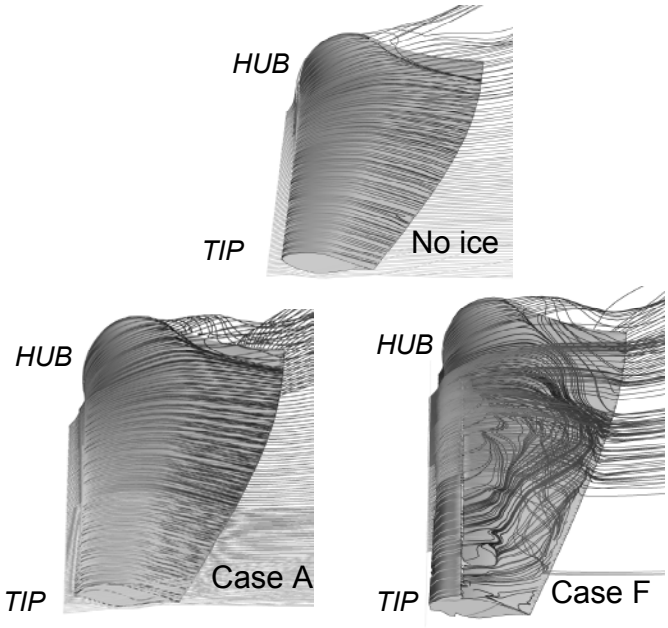

Figure 12: streamlines over the blade for Cases A & F compared to no ice.

4 Discussion

4.1 Non-"extreme" ice

It is found that ice typical of that which occurs at the wind turbine at the Alpine Test Site Gütsch does not cause significant losses in power and Annual Energy Production. The actual losses in power of the Gütsch turbine are, however, much larger. This can be seen in the comparison between the manufacturer's power curve and the actual power curve in Figure 13 (data obtained from Meteotest). The data is corrected for density for comparison to the manufacturer's power curve at standard conditions and the velocity is taken from a metrological station 150 m upstream of the turbine. The standard IEC method of bins [13] and the measured wind speed frequency distribution over a year are used to derive the actual power curve. The differences between the manufacturer's and actual power curves show a loss of Annual Energy Production of 23% (from 986 MWh to 785 MWh). These large losses in AEP cannot be attributed to the presence of ice represented by Cases A-E since this only accounts for up to 2% losses in AEP as shown above in Section 3.1. Thus for the wind turbine at Gütsch, these losses must be due to other reasons. As this wind turbine is in complex terrain, effects such as high turbulence and wind gusts are thought to be a source of losses, and are currently being investigated further in the ETH Zurich sub-scale facility.

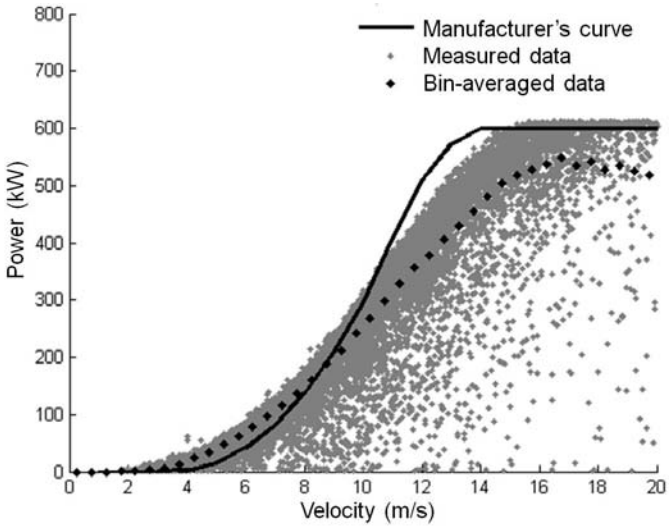

Figure 13: power measurements at Gütsch (grey dots) and the bin-averaged power curve (black dots) compared to the manufacturer`s power curve (black line).

4.2 "Extreme" ice

It is found that "extreme" ice shapes that are large enough to cause flow separation over the entire blade span can reduce the AEP by an order of 20%. These ice shapes may be expected to form at altitudes in the range 800 – 1500 m such as the Bern Jura due to the particular combination of air density and humidity. It is thus key for wind farm developers to be able to predict the likelihood of "extreme" ice forming on the blades at planned locations. The next steps of this study are therefore to (i) define quantitatively the characteristics of "extreme" ice and (ii) combine this definition with an icing event prediction model such as the Weather Research & Forecasting model of Meteotest. Icing event prediction models are required because the likelihood of icing events depends on a number of different factors. For example, even though the Gütsch site is at an altitude of 2,331 m, only small amounts of ice form on the blades. However, the Grenchenberg site is at a lower altitude of 1,350 m and subject to "extreme" icing due to the particular combination of temperature and humidity conditions there. Ultimately it is anticipated that this work will result in a predictive tool that developers of wind energy projects located in regions that are highly susceptible to icing can use for project development.

5 Conclusions

The sub-scale model wind turbine test facility at ETH Zurich has been developed to test dynamically scaled models at near full-scale non-dimensional parameters. In order to accomplish this, a novel method for performance measurements has been developed. The unique capabilities of this facility are demonstrated in a study of the effect of icing on wind turbine performance.

- Ice formed at conditions representative of the Alpine Test Site Gütsch (altitude 2,330 m) can reduce the Annual Energy Production by up to 2% (non-"extreme" icing), whereas at lower altitudes (800 – 1,500 m typical of the Bern Jura) the Annual Energy Production can be reduced up to 17% ("extreme" icing).

- The classification of possible icing events into these two different types would help the development of a more reliable predictive tool for the project development of wind farms located in regions that are highly susceptible to icing.

- For ice typical of that at high altitudes, the ice on the outboard 5% of the blade has the most significant impact on performance. Thus, ice removal or prevention systems could be substantially more efficient if their effectiveness was tailored for the outboard 5% of the blade.

Acknowledgements

The authors would like to thank the Swiss Federal Office of Energy for supporting this project (BFE-102744). The advice & model inputs at the Gütsch site provided by Silke Dierer (Meteotest) and the support & provision of the measurement data at Gütsch by René Cattin (Meteotest) are greatly appreciated, as well as the technical contributions of Hans Suter, Thomas Künzle, Claudio Troller and Cornel Reshef (ETHZ).

References

[1] Barber, S., Chokani, N. and Abhari, R.S., "Assessment of wind turbine power performance at the alpine test site Gütsch," *13th International Workshop on Atmospheric Icing of Structures*, 2009, Andermatt, Switzerland.

[2] Broeren, A.P., Bragg, M.B. and Addy, H.E., "Flowfield measurements about an airfoil with leading-edge ice shapes," *J. Aircraft*, 2006, 43(4), 1226-1234.

[3] Bragg, M., Broeren, A., Addy, H., Potapczuk, M., Guffond, D. and Montreuil, E., "Airfoil ice-accretion aerodynamics simulation," *AIAA Paper No. 2007-0085*, 2007.

[4] Bose, N., "Icing on a small horizontal-axis wind turbine – Part 1: Glaze ice profiles," *J. Wind Eng. Ind. Aero.*, 1992, 45, 75-85.

[5] Brahimi, M.T., Chocron, D. and Paraschivoiu, I., "Prediction of ice accretion and performance degradation of HAWT in cold climates," *AIAA Paper No. 98-0026*, 1998.

[6] Giguere, P. and Selig, M.S., "Design of a tapered and twisted blade for the NREL combined experiment rotor," *NREL Technical Report No. SR-500-26173*, 1999.

[7] Skamarock, W.C., Klemp, J.B., Dudhia, J., Gill, D.O., Barker, D.M., Wang, W. and Powers, J.G., "A description of the advanced WRF version 2," *Technical Note No. NCAR/TN-468+STR*, 2005, National Center for Atmospheric Research, Boulder, CO.

[8] Rae, W.H., Pope, A. and Barlow, J.B., *Low-Speed Wind Tunnel Testing*, Wiley, New York, USA, Chap. 10, 1999.

[9] Anderson, J.D., *Fundamentals of Aerodynamics*, McGraw-Hill Inc., New York, USA, Chap. 4, 1991.

[10] Schlichting, H., *Boundary-layer theory*, Springer Verlag, Berlin, Germany, Chap. 21, 2000.

[11] Tangler, J., "The nebulous art of using wind-tunnel airfoil data for predicting rotor performance," *NREL Technical Report No. CP-500-31243*, 2002.

[12] Hau, E. *Wind Turbines*, Springer Verlag, Berlin, Germany, Chap. 5, 2006.

[13] IEC Wind Turbine Generator Systems, Part 12: Power Performance Measurement Techniques, *IEC International Standard 61400-12*, 1998.